

Virilization of the Broad Line Region in Active Galactic Nuclei – connection between shifts and widths of broad emission lines

S. Jonić¹ • J. Kovačević-Dojčinović¹ • D. Ilić² •
L. Č. Popović^{1,2}

© Springer-Verlag ••••

L.Č. Popović: lpopovic@aob.bg.ac.rs

Abstract

We investigate the virilization of the emission lines H β and Mg II in the sample of 287 Type 1 Active Galactic Nuclei taken from the Sloan Digital Sky Survey database. We explore the connections between the intrinsic line shifts and full widths at different levels of maximal intensity. We found that: (i) H β seems to be a good virial estimator of black hole masses, and an intrinsic redshift of H β is dominantly caused by the gravitational effect, (ii) there is an anti-correlation between the redshift and width of the wings of the Mg II line, (iii) the broad Mg II line can be used as virial estimator only at 50% of the maximal intensity, while the widths and intrinsic shifts of the line wings can not be used for this purpose.

Keywords AGN - BH Mass - Gravitational Redshift

1 Introduction

It is widely accepted that the center of Active Galactic Nuclei (AGN) consists of a supermassive black hole (BH) surrounded by an accretion disk gravitationally bound to the BH. The accretion disk is surrounded by an optically thick gaseous region - the Broad Line Region (BLR) that emits the Broad Emission Lines (BELs) (Osterbrock 1989; Krolik 1999; Peterson 2003;

Popović 2006, 2007; Ilić et al. 2012), observed in Type 1 AGN.

The BLR is ionized by the continuum radiation from the accretion disk and is influenced by the gravitational field of the central BH. This region most likely has a complex structure (Brotherton et al. 1994; Corbin & Bronson 1996; Sulentic et al. 2000; Popović et al. 2004; Ilić et al. 2006; Hu et al. 2008). According to the one possible model of the BLR, the so-called two-component model, this emission region probably consists of two kinematically and geometrically different regions - the Very Broad Line Region (VBLR) that contributes to the broad line wings and which is closer to the BH, and the Intermediate Line Region (ILR), in which the broad line core is formed and which is further away from the BH (Sulentic et al. 2000; Popović et al. 2004; Bon et al. 2006; Hu et al. 2008; Bon et al. 2009a,b; Kovačević et al. 2010, etc). One theoretical explanation for this decomposition can be the contribution of the disk emission to the line wings (see e.g. Popović et al. 2004; Bon et al. 2009a), where the VBLR component represent the rough approximation of the disk emission. However, there are also other possible models of the BLR with different geometry (see e.g. Netzer & Marziani 2010), and here we choose to use the two-component model.

There are several methods that can be used to estimate central BH mass in a galaxy (for review see Marziani & Sulentic 2012; Shen 2013; Peterson 2014; Ilić & Popović 2014). For Type 1 AGN, the most appropriate methods for the BH mass estimation are those which use the strong broad emission lines, as e.g. the reverberation mapping (Blandford & McKee 1982; Koratkar & Gaskell 1991; Kaspi et al. 2000, 2005; Peterson et al. 2004, etc).

This method is based on the monitoring of the variations of the continuum and BEL fluxes. The time lag between these variations can be measured and in

S. Jonić

J. Kovačević-Dojčinović

Astronomical Observatory, Volgina 7, 11060 Belgrade, Serbia

D. Ilić

L. Č. Popović

Department of Astronomy, Faculty of Mathematics, University of Belgrade, Studentski trg 16, 11000 Belgrade, Serbia

that way, the photometric radius of the BLR can be estimated (see e.g. Shapovalova et al. 2009; Peterson 2014). Then, the mass of the BH can be calculated using this radius and the width of the line, which gives the velocity of the BLR, assuming that the BLR gas is virially bounded to the BH (Gaskell 1988). Similarly, $R - L$ relationship (Wandel et al. 1999; Kaspi et al. 2000; Bentz et al. 2006), which is one of the outcomes of the reverberation mapping, enables the estimation of the photometric radius, and thus of the BH mass, from only one epoch spectrum (see Laor 1998; Vestergaard & Peterson 2006; Kollmeier et al. 2006).

The basic assumption of these methods is that the BLR gas is virialized, i.e. that the main broadening mechanism is the Keplerian motion around the supermassive BH. Taking into account that the BLR geometry can be complex (see e.g. Sulentic et al. 2000; Popović et al. 2004; Gaskell 2009, etc), there are many open questions that can be very important for the applicability of those methods. The most important questions are whether the virial assumption is correct for all BELs used in these methods, and is this assumption correct in general for all AGN population?

There is an evidence supporting the virial assumption in at least several AGN for which reverberation mapping have been performed (Gaskell 1988; Kollatschny 2003a; Peterson et al. 2004; Bentz et al. 2010; Afanasiev & Popović 2015, etc). Some results imply that the virial relationship is tighter for velocity dispersion of emission lines, than for the Full Width at Half Maximum (FWHM), since the FWHM is more influenced by the line asymmetry (Peterson et al. 2004; Collin et al. 2006).

The lines which are the most frequently used as virial estimators are $H\beta$ and Mg II λ 2800 Å (see Marziani & Sulentic 2012). The $H\beta$ line is present in optical part of AGN spectra and it has smaller asymmetries and shifts than other BELs, which is the reason why $H\beta$ is mostly discussed as a BH mass estimator. At larger redshifts, $z \approx 3.7$, the $H\beta$ line is redshifted to the IR part of the spectrum. Therefore, in order to estimate BH masses, one needs prominent BELs in the UV part, that are, at higher redshifts, moved to the optical. The two strongest and mostly used UV lines are Mg II λ 2800 Å and C IV λ 1549 Å (McLure & Jarvis 2002). It seems that the C IV line is actually not a safe virial estimator of BH masses (Netzer et al. 2007; Sulentic et al. 2007; Marziani & Sulentic 2012), because C IV often shows blueshifts and asymmetries that are interpreted as winds or outflows (Gaskell 1982; Gaskell & Goosmann 2013; Marziani et al. 2013a). Marziani et al. (2013a) showed that the Mg II line can be used for BH mass esti-

mations in case of 80-90% high redshift quasars. The reverberation mapping is done only for $H\beta$, but the Mg II width can be used as a substitute for the $H\beta$ width, with certain calibrations (see Vestergaard & Osmer 2009; Shen & Liu 2012; Trakhtenbrot & Netzer 2012). However, both lines, $H\beta$ and Mg II show complex profiles, which must be taken into account, if they are used as virial estimators (see Marziani & Sulentic 2012; Marziani et al. 2013a). Marziani & Sulentic (2012) pointed out that $H\beta$ in a fraction of AGN with a large FWHM $H\beta$ (Population B, FWHM $H\beta > 4000$ km/s) is not the good virial estimator because of the redshifted VBLR component, while Marziani et al. (2013b) found that a fraction of AGN with small FWHM $H\beta$ (Population A), may have a blueshifted, non-virial component in Mg II, probably caused by an outflow.

On the other hand, one more method, rarely used for the BH mass estimation, is based on the gravitational redshift of the BELs, which should be an indicator of the BH gravity (see Zheng & Sulentic 1990; Popović et al. 1995; Kollatschny 2003b). Since the BLR is stratified, the broad line wings are probably arising in the deeper parts of the BLR, closer to the BH. It is possible that, at least in the line wings, the relativistic effect could be strong enough to be measured. Zheng & Sulentic (1990) proposed that the systemic redshift of the $H\beta$ wings, relative to the line core, seen in the Population B AGN, can be caused by the gravitational redshift.

Here we investigate the virilization in the BLR, exploring the $H\beta$ and Mg II line widths at 5%, 10% and 50% of the intensity maximum and corresponding shifts of their centroids with respect to the broad line peak. We are starting from the hypothesis that if there is a dominant Keplerian motion affecting the line widths, there should exist the gravitational redshift in the line profile. We use the statistics of the large AGN sample to check the relationships between the widths and the shifts within the lines.

The paper is organized as following: In Section 2 we present our assumptions about the gas virilization, in Section 3 we describe the sample selection, spectra decomposition and analysis. The results are given in Section 4, and discussed in Section 5. Finally, in Section 6 we outline our conclusions.

2 The virilization in the emission gas

If the emitting gas is virialized, it is expected that the dominant line broadening is due to the Keplerian motion of the gas. Also, if the mass of the central source is

large enough, the gravitational redshift is expected to be seen in BELs, or at least in the line wings, since the line wings are originating closer to the BH, so the influence of the BH gravity is stronger. If the emission gas in the BLR is virialized, one can expect to observe correlations between the widths and gravitational redshifts of the BELs.

From the virial theorem, the mass of the BH can be estimated as (Peterson et al. 2004):

$$M = f \frac{R v^2}{G}, \quad (1)$$

where G is the gravitational constant, R is the BLR radius, v is the velocity of the gas in the BLR, and f is the virial factor which depends on the BLR geometry and inclination. The FWHM of the BELs can be used to measure the mean gas velocity (v) in the BLR.

On the other hand, the redshift caused by the gravitational field, can give us an upper limit of the BH mass as (Zheng & Sulentic 1990):

$$M = \frac{c^2 R}{G} z_G, \quad (2)$$

where z_G is the gravitational redshift of the emission line.

Assuming that in both equations (1) and (2) R represent the photometric radius, we can obtain the expected relationship between z_G and FWHM of the line:

$$z_G \sim FWHM^2. \quad (3)$$

Therefore, if the virial assumption is valid, we can expect that there is a power law dependence between the gravitational redshift and gas velocity, with exponent $n = 2$. For FWHM, the corresponding z_G is Δz_{50} , that is intrinsic redshift of the line, measured as a centroid shift at half maximum with respect to the broad line peak (for more details see Sec 3.3). Consequently, there should be a linear correlation between logarithms of FWHM and Δz_{50} , $\log(\Delta z_{50}) = C \log(FWHM)$, where C is a constant. Both parameters are given in km/s.

Note that at higher velocities (widths at 10 % and 5 % of line maximum), we also expect a relationship like equation (1) although this has not been proven observationally. We do not have to know f for these velocities, only to assume it is the same for all objects where the BLR is virialized. Therefore, we expect the same relationship (equation 3) of these widths with corresponding intrinsic redshifts measured at 10 % and 5 % of line maximum.

3 Sample and Analysis

3.1 The AGN Sample

For this research we used spectra from the Sloan Digital Sky Survey (SDSS) database, Data Release 7. We choose the sample with the broad H β and Mg II $\lambda 2800$ Å lines (their equivalent widths requested to be larger than zero) in the redshift range $0.407 \leq z \leq 0.643$. This sample of 293 AGN is initially used for research of the relations between the UV and optical Fe II emission in the Type 1 AGN, so the detailed search criteria and fitting procedures are given in Kovačević-Dojčinović & Popović (2015). After eliminating the spectra with very noisy UV part, near the Mg II line, our sample contained 287 AGN spectra.

Since in this investigation we search for the gravitational redshift in the lines, we measure the intrinsic shifts in the whole sample (see Section 3.3), and we eliminate all spectra with blueshifted H β /Mg II profiles. In these spectra, some other effects (as e.g. outflows), could be more dominant than the gravitational effects, so they are not convenient for this research. Therefore, we further investigate one subsample of 209 spectra in which H β lines have no blueshift, and another subsample of 150 spectra in which there is no blueshift in the Mg II lines. Finally, to compare the properties between these two lines, we use a third subsample of 123 spectra in which both lines have no blueshift. We should note here that with this selection, the large number of spectra are rejected from the initial sample. However, it is difficult to state that we have completely eliminated all spectra with strong outflow influence, since it is possible that the combination of the outflow and gravitational redshift produce symmetrical line shape.

3.2 Line Fitting Procedure

In order to test the virialization in the broad H β and Mg II $\lambda 2800$ Å lines, it is very important to remove all overlapping lines, and to obtain the clear BELs profiles.

The complex shapes of BELs profiles indicate that different parts of BELs are coming from different emission regions. Since we assume that the Doppler broadening, caused by the motion of the emitting clouds, dominates in the line profiles of AGNs, we model the emission lines with the sum of Gaussians, where we suppose that each Gaussian represents the emission from kinematically different emission region. Therefore, the kinematical and physical properties of each emission region are reflected in the shifts, widths and intensities of Gaussians. In the case of the broad Balmer lines, we find that the best fit is obtained using the two Gaussians (see e.g. Bon et al.

2009a; Kovačević et al. 2010), which supports the two-component model of the BLR (Popović et al. 2004; Bon et al. 2006; Hu et al. 2008). The detailed description of this multi-Gaussian model and the fitting procedure is given in Kovačević-Dojčinović & Popović (2015), where fitting of this sample is performed in two spectral ranges: UV (2650-3050) and optical (4000-5500).

In the case of the optical range which includes the $H\beta$ line, we subtract the continuum emission using the continuum windows given in Kuraszekiewicz et al. (2002). Since the $H\beta$ line overlaps with the optical Fe II lines, He II and [O III] $\lambda\lambda$ 4959, 5007 Å narrow lines, we apply the multi-Gaussian fitting model (see Fig 2. in Kovačević et al. 2010), to extract only the broad profile of $H\beta$. The $H\beta$ line is fitted with three Gaussians: one represents the emission from the NLR, and other two from the BLR. We assume that the Gaussian which fits the line wings represents the emission from the parts of the BLR closer to the BH (VBLR) and the one which fits the line core, the emission from the outer parts of the BLR (ILR). The [O III] lines have the same width and shift as the $H\beta$ narrow component, because we assume they all originate in the NLR. Additionally, the [O III] lines have one more component which describes the asymmetry in the wings of these lines. Numerous optical Fe II lines are fitted with the Fe II template¹ presented in Kovačević et al. (2010) and Shapovalova et al. (2012).

In the case of Mg II, the most challenging is to remove the numerous UV Fe II lines which overlap with Mg II. In order to fit the UV part of the spectra, first the UV Balmer pseudo-continuum has to be subtracted. We use the UV Balmer pseudo-continuum model presented in Kovačević et al. (2014). After that, we fit simultaneously the UV Fe II lines in the range 2650-3050 Å with the Mg II line. For the UV Fe II lines we use the model described in Popović et al. (2003) and Kovačević-Dojčinović & Popović (2015). Note that the Mg II line is the resonant doublet Mg II $\lambda\lambda$ 2795, 2803 Å. However, it can not be resolved since the components are very broad and overlap. Therefore, we fit the Mg II line as a single line, with two Gaussian components, one which fits the core, and one which fits the wings of the line. The example of the spectrum decomposition near $H\beta$ and Mg II are given in Figure 1.

There are various BLR models which predict the use of different functions, as e.g. Lorentzians or power-law functions, for fitting the emission line profiles in AGNs. In this work, we use the multi-Gaussian fitting decomposition only to remove the overlapping lines and to reproduce the broad line profile of $H\beta$ and Mg II, which

are obtained as the sum of the core and wing broad Gaussian. Since the parameters of this fitting decomposition are not used furthermore in this investigation, the results are not strongly affected with the function used for the line profile fitting.

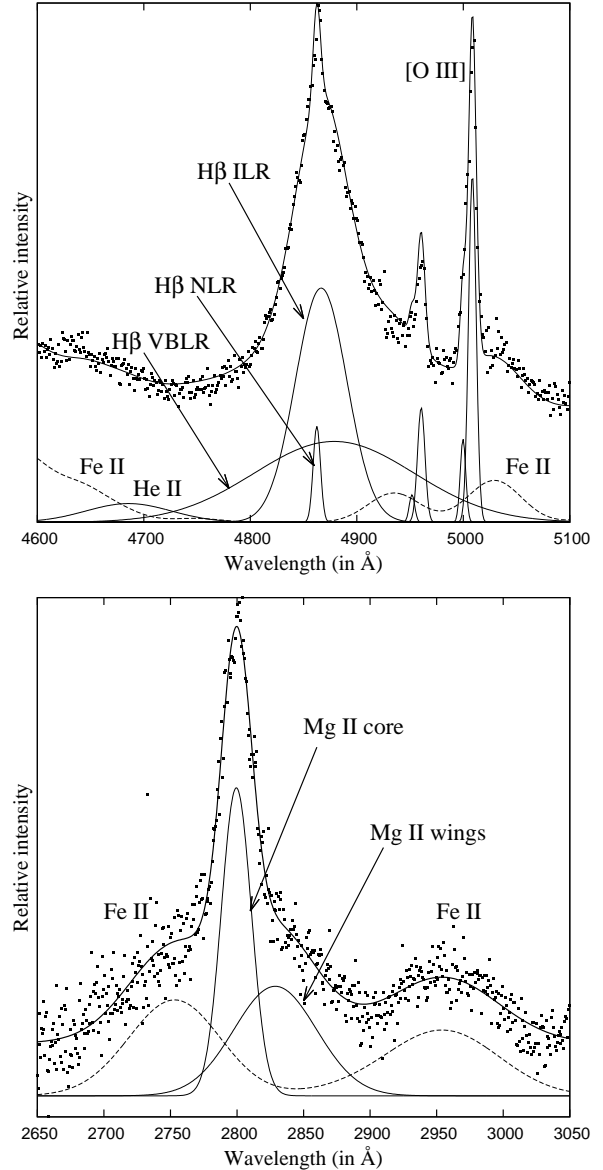


Fig. 1 The example of the spectra decomposition for object SDSS J032205.04+001201.4, near $H\beta$ (top) and Mg II line (bottom). The broad $H\beta$ and Mg II lines are decomposed into two components which fit the line core and the line wings. The iron lines are denoted with dashed line.

3.3 Measuring the widths and the intrinsic line shifts

In order to measure the line widths and intrinsic shifts of the broad $H\beta$ and Mg II, we extract only the broad component from the composite $H\beta$ and Mg II lines.

¹http://servo.aob.rs/FeII_AGN/

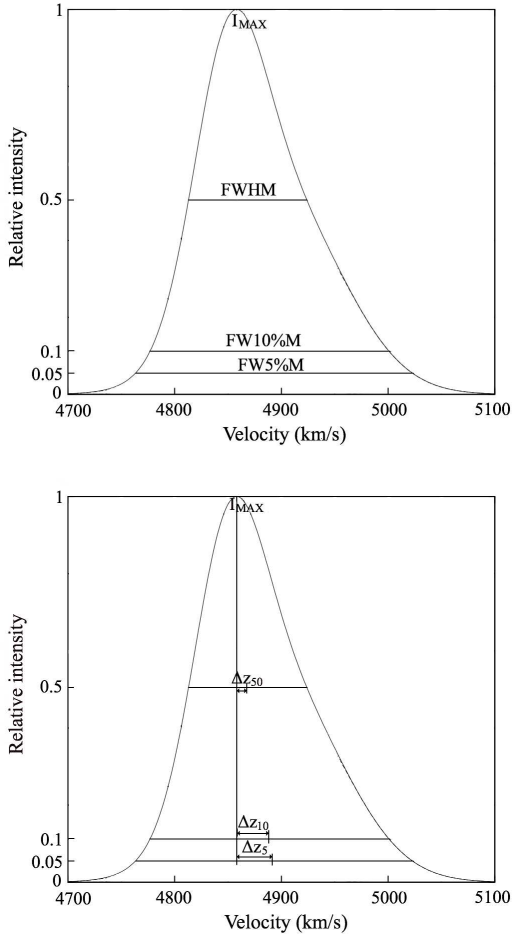


Fig. 2 The example of the line width (top) and intrinsic redshift measurements (bottom) of the broad (VBLR+ILR) component of $H\beta$. The widths are measured at 50%, 10% and 5% of the maximum (FWHM, FW10%M and FW5%M). The intrinsic redshifts (Δz_{50} , Δz_{10} and Δz_5) are measured as a difference between the centroid shift and the broad component peak, at 50%, 10% and 5% of the line maximum.

The fitting procedure enables us to remove all overlapping lines, such as optical Fe II, He II, [O III] and $H\beta$ NLR in the case of $H\beta$, so the sum of the ILR and VBLR $H\beta$ components represents the clear broad $H\beta$ profile (see Figure 1, top). In the case of Mg II, after removing the UV Fe II, the broad profile of Mg II consists of two Gaussians (see Figure 1, bottom). We measure the FWHM for both lines, as well as Full Width at 10% of the maximum (FW10%M) and the Full Width at 5% of the maximum (FW5%M). The example of the line width measurements at different levels of line intensity is shown in Figure 2 (top).

The intrinsic shift of the line is measured at different levels of the line intensity (at 50%, 10% and 5%), as a centroid shift with respect to the broad line peak, as

it is shown in Figure 2 (bottom). The intrinsic shift measured at 50% of the line maximal intensity (I_{MAX}) is then:

$$\Delta z_{50} = z_{50} - z_{I_{MAX}}, \quad (4)$$

where $z_{I_{MAX}}$ is the shift of the broad line peak, i.e. the maximum of the line intensity relative to the central wavelength, z_{50} is the same but for the centroid at 50% of the I_{MAX} . Similarly, the intrinsic shifts at the 10% and 5% of the I_{MAX} are given as:

$$\Delta z_{10} = z_{10} - z_{I_{MAX}}, \quad (5)$$

$$\Delta z_5 = z_5 - z_{I_{MAX}}, \quad (6)$$

where z_{10} and z_5 are the shifts of the centroid at 10% (5%) of the I_{MAX} , relative to the broad line peak.

4 Results

To check the virialization of the broad $H\beta$ and Mg II lines, we analyze the relationships between their widths and intrinsic shifts. These parameters are measured at different levels of the line intensity (at 50 %, 10 % and 5 % of I_{MAX}) and compared within one line and between $H\beta$ and Mg II.

For the $H\beta$ line, the measured shifts in the whole sample of 287 AGN are within the range from -445 km s^{-1} to 1045 km s^{-1} at 50% of the I_{MAX} , from -1151 km s^{-1} to 3179 km s^{-1} at 10% of the I_{MAX} and from -1469 km s^{-1} to 3897 km s^{-1} at 5% of the I_{MAX} . In case of the Mg II line, these values are within the range from -206 km s^{-1} to 1410 km s^{-1} at 50% of the I_{MAX} , from -2771 km s^{-1} to 3678 km s^{-1} at 10% of the I_{MAX} and from -5224 km s^{-1} to 3678 km s^{-1} at 5% of the I_{MAX} .

We find that for the broad $H\beta$ line, the line width is well correlated with the line intrinsic shift, measured at all intensity levels. For 50 % of line intensity, the correlation between the FWHM and Δz_{50} is $\rho \approx 0.70$, $P < 0.00001$. Significant correlations are found also for the 10% and 5% of line intensity (FW10%M vs. Δz_{10} , $\rho \approx 0.60$, $P < 0.00001$, FW5%M vs. Δz_5 , $\rho = 0.58$, $P < 0.00001$). The correlations are shown in Figure 3. The correlation coefficients between the widths and redshifts for the $H\beta$ and Mg II lines are listed in Table 1.

In the case of the Mg II line, a correlation between the Mg II width and line intrinsic shift is present only for 50 % of the line intensity with $\rho = 0.59$, $P < 0.00001$.

However, it is interesting that for the 10 % and 5 % of the Mg II intensity, the correlation between the Mg II width and line intrinsic shift becomes opposite (see Figure 4), with $\rho = -0.62$, $P < 0.00001$ for 10 % of the line intensity, and $\rho = -0.68$, $P < 0.00001$ for 5 % of the line intensity.

We analyze the relationships between the widths of the H β and Mg II lines, measured at different levels of the line intensity. The results are shown in Figure 5 and Table 2. While there is a good correlation between the FWHMs of these lines ($\rho = 0.68$, $P < 0.00001$), there are no correlations between their FW10%Ms and FW5%Ms. Similar trend is seen for the line shifts: there is a correlation between the shifts of the lines at 50 % of the intensity (Δz_{50} H β vs. Δz_{50} Mg II, $\rho = 0.42$, $P < 0.00001$), while there are no correlations between the Δz_{10} (or Δz_5) of H β and Mg II (see Figure 6 and Table 2).

The measured values of the FWHMs, FW10%Ms, FW5%Ms and corresponding shifts of H β and Mg II, for the complete sample of 287 AGN, are given in Tables 3 and 4, in Appendix.

It is hard to estimate the errors in the measured shifts and widths, since both, fitting procedure and S/N of a spectrum, are contributing. Since continuum subtraction probably has a large influence on the error, we make a test with an underestimate and overestimate of the underlying continuum level for 3% in the complete sample, and repeat the fitting procedure for H β . We find that for Δz_{50} the mean discrepancy with previous measurement is $\sim 20\text{km s}^{-1} \pm 100\text{km s}^{-1}$, while for the FWHM it is $\sim 200\text{km s}^{-1} \pm 390\text{km s}^{-1}$. For the widths and shifts measured at 10% and 5% of the I_{MAX} , the errors are larger. Nevertheless, the correlations between the shifts and widths found for the 10% and 5% of I_{MAX} in the case of H β remain consistent. For FW10%M vs. Δz_{10} they are $\rho = 0.58$, $P < 0.00001$ and $\rho = 0.55$, $P < 0.00001$, for 3% higher and 3% lower continuum level respectively. In the case of FW5%M vs. Δz_5 , the correlations are: $\rho = 0.49$, $P < 0.00001$ and $\rho = 0.52$, $P < 0.00001$, respectively.

4.1 The functional dependence between widths and intrinsic shifts

We investigate the possible functional dependence of the H β and Mg II line widths and intrinsic shifts. If the line widths and the intrinsic shifts are dominated by the gravitation of the BH, we expect that these parameters are linked with a function of the form $Y = m \cdot X^n$ (see Section 2, equation 3).

Therefore, we fit widths vs. shifts of H β and Mg II, with $Y = m \cdot X^n$, where $X = FWHMs$, and $Y = \Delta z_{50}$.

The same is done for the widths and shifts measured at 10% and 5% of the maximal intensity. The results are presented in Table 1 and Figure 7.

In the case of the H β line, the fit gives the exponent which is in agreement with the theoretical value of $n = 2$, within the error-bars (see Table 1). The agreement is slightly better for the widths and shifts measured at 50% of I_{max} ($n = 1.85 \pm 0.19$). However, in the case of Mg II, the exponent which is in agreement with the theoretical value is obtained only for the widths and shifts measured at 50% of I_{max} ($n = 2.06 \pm 0.27$), while for the 10% and 5% of I_{max} , the exponent is $n < 0$ (see Table 1).

In order to find more accurate relationships between widths and shifts of H β and Mg II, we perform the same fitting for the subsample of 123 AGN, where both lines, H β and Mg II, are redshifted (see Sec 3.1). The results are shown in Figure 8, and in Table 1.

5 Discussion

Since the broad H β and Mg II lines are widely used as virial estimators of AGN BH masses, it is important to investigate their applicability for that purpose, and to check whether the intrinsic redshifts of these lines represent gravitational redshifts, i.e. could they be used as good virial estimators.

There is the evident difference in the profiles of the Mg II and H β lines. Kovačević-Dojčinović & Popović (2015) compared the average widths of Gaussians which fit the core and the wings of the Mg II and H β , and found that the core of Mg II is slightly narrower than the core of H β , while wings of the Mg II are significantly broader than the H β ones. Furthermore, there is a correlation between the Mg II and H β core widths, as well as between their shifts, while there is no correlation between the kinematical properties of their wings (Kovačević-Dojčinović & Popović 2015). This implies that their cores probably originate from the kinematically connected regions, while this can not be stated for their wings. In our sample of 287 objects, there are only 123 AGN which have no blueshift in H β and Mg II. Some objects have a blueshift in one of these two lines, which means that if one of these two lines is a good virial estimator for one object, the other line can be strongly influenced by some other effects beside the gravitational, and could not be taken as a good virial estimator. This implies as well that emission in wings of these lines probably originate from kinematically different emission region.

Considering only the AGN subsamples with redshifted H β or Mg II, we find expected linear correlations

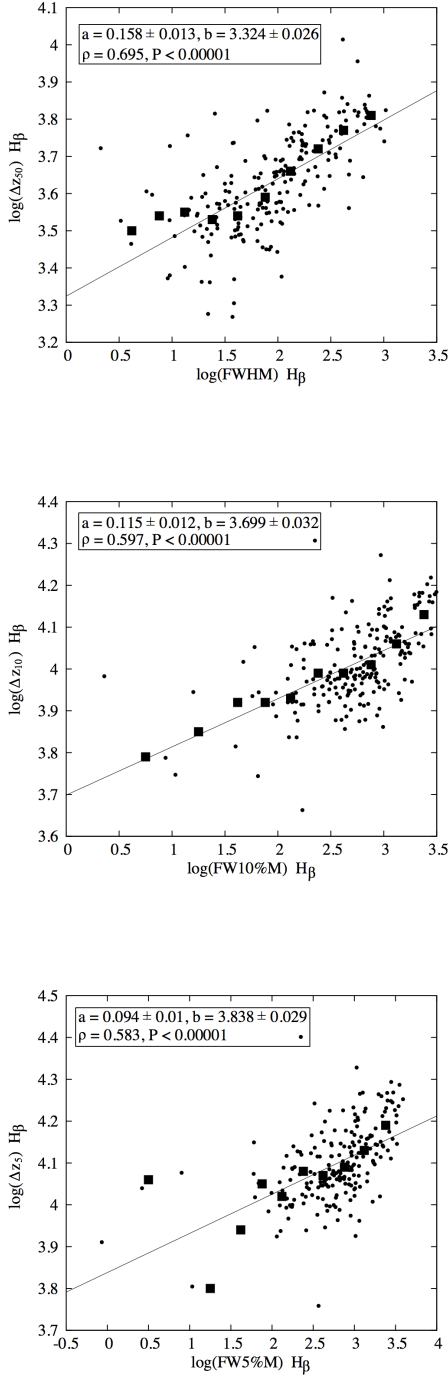


Fig. 3 Correlation between the widths and intrinsic shifts of the broad $H\beta$ lines (given in km/s), measured for 50 % I_{\max} (top), 10 % I_{\max} (middle), and 5 % of the I_{\max} (bottom). Data are fitted with a linear function: $Y = a + b \cdot X$. The coefficients a and b , as well as Spearman coefficient of correlation (ρ) and P-value are shown on plots. The binned values are assigned with black squares.

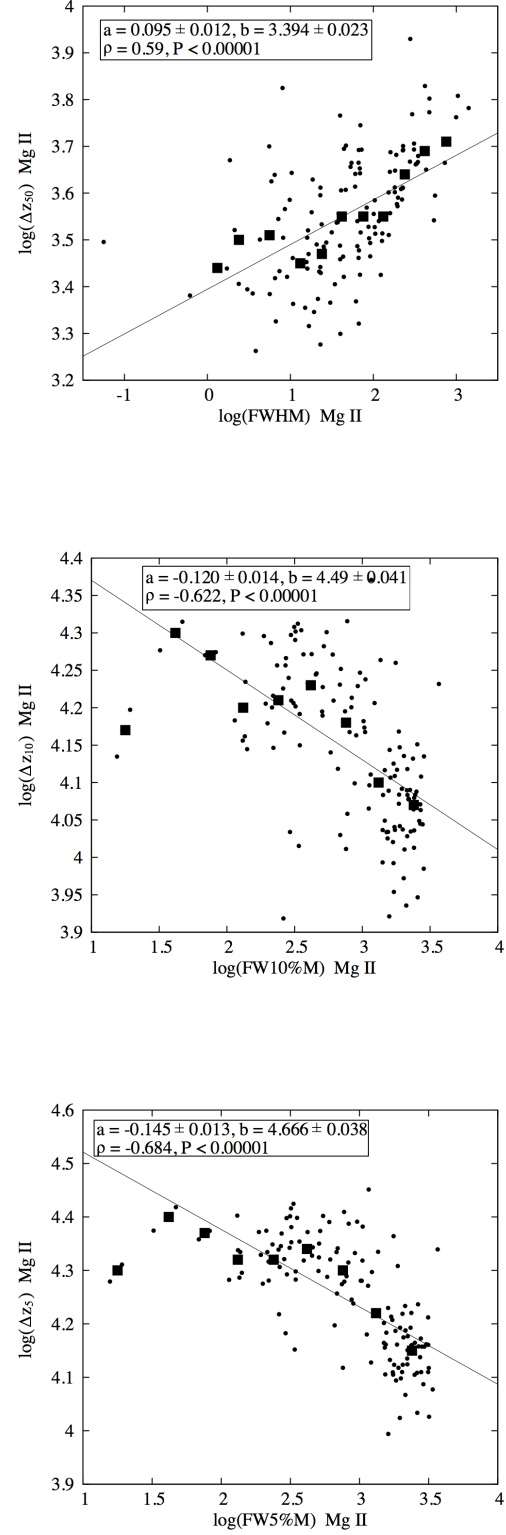


Fig. 4 The same as in Figure 3 but for Mg II.

between logarithms of the FWHMs and Δz_{50} for both lines, which implies that the intrinsic redshifts are indeed connected with the gravitational redshift of these lines. However, while correlation between FWHM and intrinsic redshift is significant at all levels of I_{\max} for $H\beta$, for Mg II the anti-correlation becomes significant for 10% and 5% of I_{\max} .

Similarly, the widths of these two lines are well correlated at 50% of the line intensity, as well as the intrinsic shifts, while there are no correlations between these parameters at 10% and 5% of I_{\max} .

The above result is confirmed with fitting of the functional dependence between the widths and shifts of these lines, as well. The theoretically predicted dependence $\Delta z_{50} = \text{const} \cdot FWHM^2$ (see Sec 2) is obtained from the best fit with the function $Y = m \cdot X^n$. The estimated n values are in agreements with predicted $n = 2$, within the error-bars for both lines, $H\beta$ and Mg II. However, while for $H\beta$ the mentioned relationship is valid also for widths and intrinsic redshifts at 10% and 5% of I_{\max} , for Mg II wings our initial assumption of the virialized gas failed. The relationships between the Mg II widths and intrinsic shifts at 10% and 5% of I_{\max} do not match the theoretical prediction.

Numerous UV Fe II lines form broad features which is hard to be distinguished from the Mg II wings. Therefore, one can suspect that the Mg II wings shape can be affected by subtraction of the Balmer continuum and UV Fe II lines which overlap with Mg II. Surely, this introduces an uncertainty for FWHM and Δz measurements close to continuum level, at 10% and 5% of I_{\max} . However, we do not expect that this uncertainty produces significant anti-correlations between widths and intrinsic shifts in the Mg II wings, which are detected ($\rho = -0.62$ and $\rho = -0.68$, $P < 0.0001$, for 10% and 5% of I_{\max}).

The blueshifts in both lines, and not applicable virial assumption in case of Mg II line wings, can be explained by outflow of the BLR gas, caused by the radiation pressure force or some other unknown mechanisms (Ilić et al. 2010).

6 Conclusions

In this paper we investigate the virialization of the broad $H\beta$ and Mg II lines in the sample of 287 type 1 AGN taken from the SDSS database. The aim of this work is to test whether the broad $H\beta$ and Mg II are indeed good virial estimators for all objects, and to check if the intrinsic redshift in these lines is connected to the gravitation redshifts, i.e. can be used for the BH mass estimation. For that purpose, we measure the widths

and intrinsic shifts of those lines, at 50%, 10% and 5% of the maximal intensity. We analyze the correlations and functional dependences between centroid redshifts and corresponding widths of those lines, and compare it with theoretically predicted relationships.

From this research we can conclude that:

1. For the AGN sample with redshifted $H\beta$ line, there are good correlations between all measured shifts and widths (at 50%, 10% and 5% of I_{\max}). Also, the theoretically expected relationship $\Delta z_{50} \sim FWHM^2$ is confirmed, within the error-bars. The same relationship is confirmed for widths and corresponding intrinsic redshifts, measured at different intensity levels (10% and 5% of I_{\max}). This implies that $H\beta$ is a good virial estimator of AGN BH masses, and that the intrinsic redshift of the $H\beta$ line is dominantly caused by gravitational effects. However, there is a group of AGN with a blue asymmetry in the broad emission lines. Therefore, to use the $H\beta$ line one should check the asymmetry of $H\beta$, and in the case of the red asymmetry, it probably can be used for the BH mass estimation, while in the case of the blue asymmetry, it should be taken with caution.
2. For the AGN sample with the intrinsic redshift in the broad Mg II line, there is the correlation between intrinsic redshift and width but only at 50% of I_{\max} . The theoretically expected relationship $\Delta z_{50} \sim FWHM^2$ is confirmed as well, but it failed for widths and intrinsic redshifts at 10% and 5% of I_{\max} . As the widths and shifts are measured closer to the continuum level in the wings of the Mg II lines, an anti-correlation between widths and corresponding redshifts begins to appear. Consequently, the Mg II line can be used as a virial estimator for AGN with the red asymmetry, but only at 50% of I_{\max} . The intrinsic redshift at that level probably can be used for the BH mass estimation. On the other hand, the widths and shifts measured in wings of these lines can not be used for this purpose. The same as for $H\beta$, in the case of the blue asymmetry, Mg II should be taken with caution as the virial estimator.
3. This research open some new questions considering the anti-correlations between gravitational redshift and widths in the wings of Mg II line. Also, the number of the Mg II lines with the blue asymmetry is larger compared to $H\beta$. It seems that the broader component of Mg II (which contribute to the line wings) is coming from the region where some other mechanisms, except the gravity cannot be neglected.

Candidates for this mechanism are gas outflows from the BLR probably caused by the radiation pressure force or accretion disk wind.

Acknowledgments

This investigation is supported by the Ministry of Education, Science and Technological Development of Republic of Serbia in the frame of Project 176001 *Astrophysical spectroscopy of extragalactic objects*. We thank to an anonymous referee for very useful comments.

References

- Afanasiev, V. L., Popović, L. Č., 2015, ApJL, 800, 35
- Bentz, Misty C., Peterson, B. M., Pogge, R. W., Vestergaard, M., Onken, C. A., 2006, ApJ, 644, 133
- Bentz, M. C., Walsh, J. L., Barth, A. J., Yoshii, Y., Woo, J.-H., Wang, X., Treu, T., et al., 2010, ApJ, 716, 993
- Blandford, R.D, McKee, C.F., 1982, AJ, 255, 419
- Bon, E., Gavrilović, N., La Mura, G., Popović, L. Č., 2009b, NewAR, 53, 123
- Bon, E., Popović, L. Č., Gavrilović, N., La Mura, G., Mediavilla, E., 2009a, MNRAS, 400, 924
- Bon, E., Popović, L. Č., Ilić, D., Mediavilla, E., 2006, NewAR, 50, 716
- Brotherton, M. S., Wills, B. J., Francis, P. J., Steidel, C. C., 1994, ApJ, 430, 495
- Collin, S., Kawaguchi, T., Peterson, B. M., Vestergaard, M., 2006, A&A, 456, 75
- Corbin, M. R., Boroson, T. A., 1996, ApJS, 107, 69
- Gaskell, C. M., 1982, ApJ, 263, 79
- Gaskell, C. M., 1988, ApJ, 325, 114
- Gaskell, C. M., 2009, NewAR, 53, 140
- Gaskell, C. M., Goosmann, R. W., 2013, ApJ, 769, 30
- Hu, C., Wang, J., Ho, L. C., Chen, Y., Bian, W., Xue, S., 2008, ApJ, 683L, 115
- Ilić, D., Popović, L. Č., 2014, JPhCS, 548, article id. 012002
- Ilić, D., Popović, L. Č., Bon, E., Mediavilla, E. G., Chavushyan, V. H., 2006, MNRAS, 371, 1610
- Ilić, D., Popović, Luka Č., Shapovalova, A. I., Burenkov, A. N., Kollatschny, W. Kovačević, A., Chavushyan, V., La Mura, G., Rafanelli, P 2012, JPhCS, 397, 2050
- Ilić, D., Popović, L. Č., Shapovalova, A. I., Kovačević, A., León-Tavares, J., Chavushyan, V. H., 2010, MSAIS, 15, 166
- Kaspi, S. Maoz, D. Netzer, H., Peterson, B. M., Vestergaard, M. Jannuzi, B. T., 2005, ApJ, 629, 61
- Kaspi, S. Smith, P. S., Netzer, H. Maoz, D. Jannuzi, B. T., Giveon, U., 2000, ApJ, 533, 631
- Kollatschny, W., 2003a, Astron. Astrophys. 407, 461
- Kollatschny, W., 2003b, Astron. Astrophys. 412, 61
- Kollmeier, J. A., Onken, C. A., Kochanek, C. S., Gould, A., Weinberg, D. H., Dietrich, M., Cool, R. et al., 2006, ApJ, 648, 128
- Koratkar, A. P., Gaskell, C. M. 1991, ApJ, 375, 85
- Kovačević-Dojčinović, J., Popović L. Č., 2015, ApJS, 221, 35
- Kovačević J., Popović L. Č., Dimitrijević M. S. 2010, ApJS, 189, 15
- Kovačević J., Popović L. Č., Kollatschny, W. 2014, ASR, 54, 1347
- Krolik, J., 1999, Active Galactic Nuclei: From the Central BH to the Galactic Environment (Princeton: Princeton Univ. Press)
- Kuraszkiewicz, J. K., Green, P. J., Forster, K., Aldcroft, T. L., Evans, O. N., Koratkar, A., 2002, ApJS, 143, 257
- Laor, A., 1998, ApJ, 505, 83
- Marziani, P., Sulentic, J. W., 2012, NewAR, 56, 49
- Marziani, P., Sulentic, J. W., Plauchu-Frayn, I., del Olmo, A., 2013, A&A, 555, 89
- Marziani, P., Sulentic, J. W., Plauchu-Frayn, I., del Olmo, A., 2013, ApJ, 764, 150
- Mc Lure, R. J., Jarvis, M. J., 2002, MNRAS, 337, 109
- Netzer, H., Lira, P., Trakhtenbrot, B., Shemmer, O., Cury, I., 2007, ApJ, 671, 1256
- Netzer, H., Marziani, P., 2010, ApJ, 724, 318
- Osterbrock, D.E., 1989, Astrophysics of Gaseous Nebulae and Active Galactic Nuclei
- Peterson, B.M., 2003, An Introduction to Active Galactic Nuclei, Cambridge University Press
- Peterson, B. M., 2014, SSRv, 183, 253
- Peterson, B.M., Ferrarese, L., Gilbert, K. M., Kaspi, S., Malkan, M. A., Maoz, D., Merritt, D., Netzer, H., Onken, C. A., Pogge, R. W., Vestergaard, M., Wandel, A., 2004, ApJ, 613, 682
- Popović L. Č., 2006, SerAJ, 173, 1
- Popović L. Č., 2007, JPhCS, 63, 2018
- Popović, L. Č. Mediavilla, E., Bon, E., Ilić, D., 2004, A&A, 423, 909
- Popović, L. Č., Mediavilla, E. G., Bon, E., Stanić, N., Kubičela, A., 2003, ApJ, 599, 185
- Popović, L. Č. Vince, I., Atanacković - Vukmanović, O., Kubičela, A. 1995, A&A, 293, 309
- Shapovalova, A. I., Popović, L. Č., Burenkov, A. N., Chavushyan, V. H., Ilić, D., Kovačević, A., Kollatschny, W., et al., 2012, ApJS, 202, 10S
- Shapovalova, A. I., Popović, L. Č., Bochkarev, N. G., Burenkov, A. N., Chavushyan, V. H., Collin, S., Doroshenko, V. T., Ilić, D., Kovačević, A., 2009, NewAR, 53, 191
- Shen, Y., 2013, Bulletin of the Astronomical Society of India, 41, 61
- Shen, Y., Liu X., 2012, ApJ, 753, 125
- Sulentic, J. W., Bachev, R., Marziani, P., Negrete, C. A. Dultzin, D., 2007, ApJ, 666, 757
- Sulentic, J.W., Marziani, P., Dultzin-Hacyan, D., 2000, ARA&A, 38, 521
- Trakhtenbrot B., Netzer H. 2012, MNRAS, 427, 3081
- Vestergaard, M., Osmer, P. S., 2009, ApJ, 699, 800
- Vestergaard, M, Peterson, B.M., 2006, ApJ, 641, 676
- Wandel, A. Peterson, B. M., Malkan, M.A., 1999, ApJ, 526, 579
- Zheng, W., Sulentic, J. W., 1990, ApJ, 350, 512

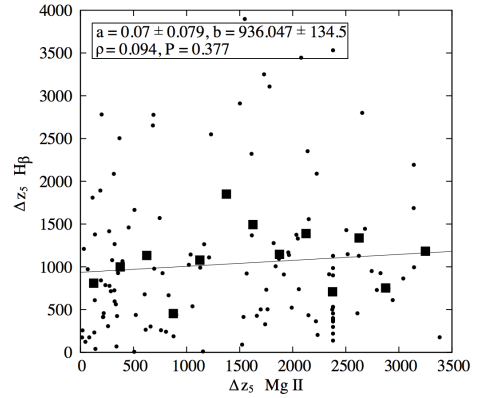
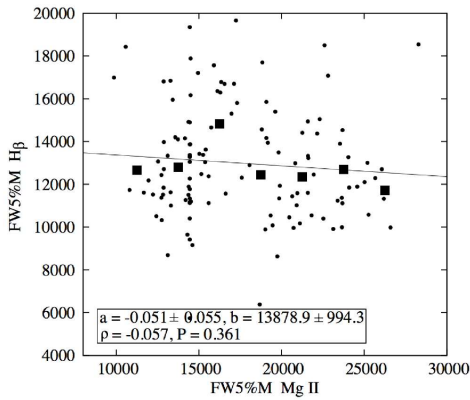
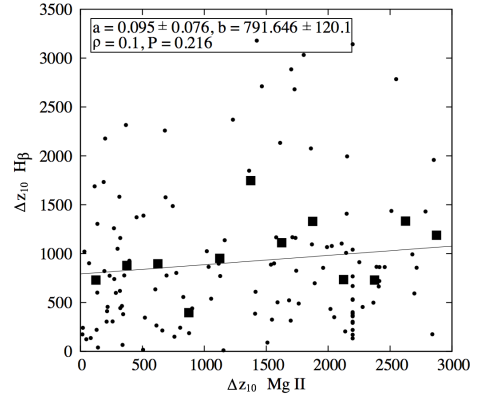
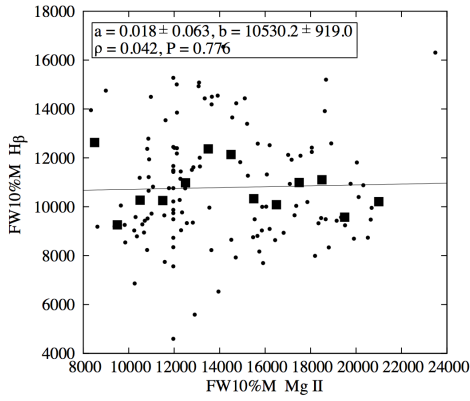
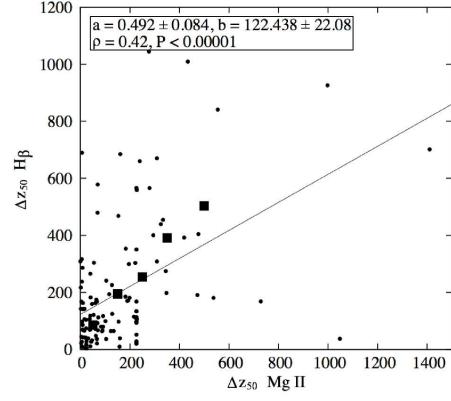
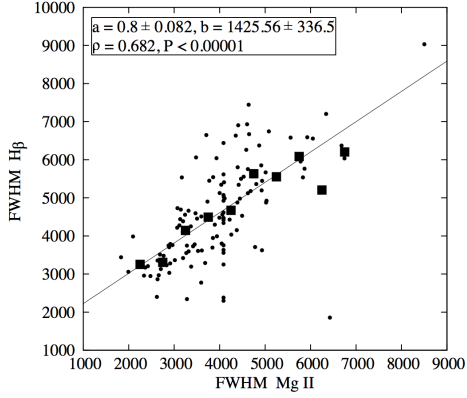


Fig. 5 Top: the correlation between the FWHMs of the $H\beta$ and Mg II lines. Middle and bottom: no correlation between the FW10%M and FW5%M of these lines. The notation is the same as in Figure 3.

Fig. 6 Top: the correlation between the redshifts Δz_{50} of the $H\beta$ and Mg II lines. Middle and bottom: no correlation between the redshifts Δz_{10} and Δz_5 of these lines. The notation is the same as in Figure 3.

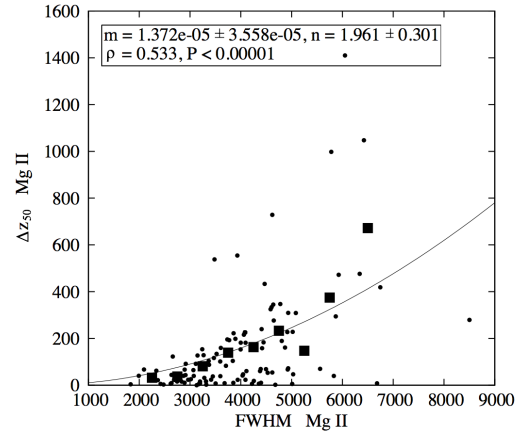
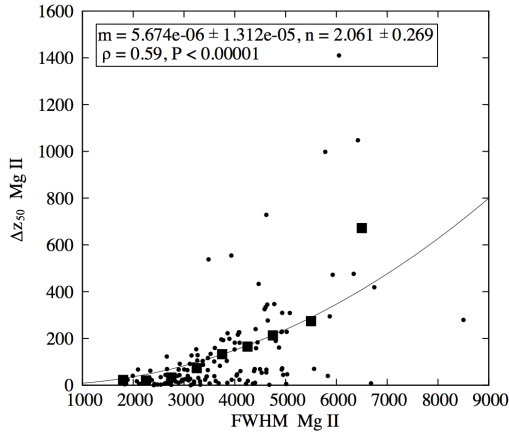
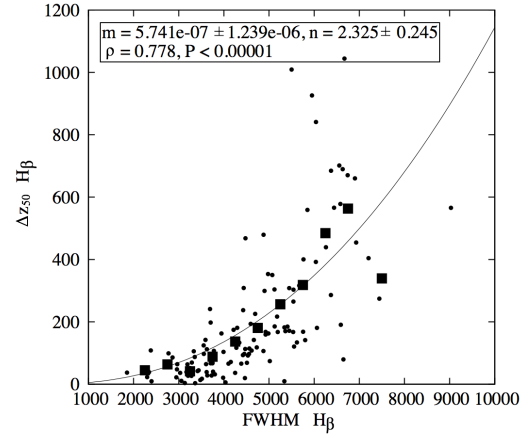
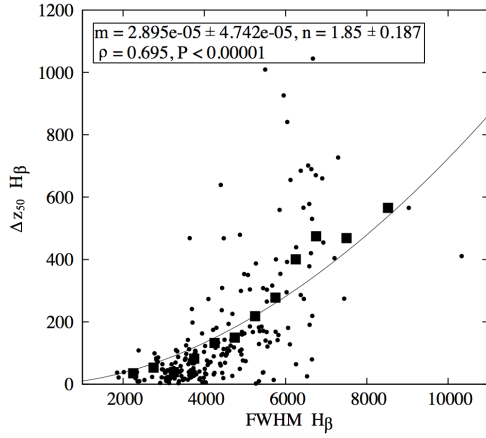


Fig. 7 Relationship between widths (km/s) and intrinsic shifts (km/s) of H β (top) and Mg II (bottom). The observations are fitted with the function: $Y = m \cdot X^n$. Binned values are shown with black squares.

Fig. 8 The same as in Figure 7, just for the subsample of 123 AGN, in which both, H β and Mg II lines, are redshifted. All spectra with the blueshift in one of these two lines are rejected.

Table 1 The widths (X) and intrinsic shifts (Y) of the H β and Mg II are fitted with function: $Y = m \cdot X^n$. The parameters m and n , obtained from the fit, as well as the Spearman coefficients of correlation (ρ) and P -values, are also listed.

widths vs. shifts	number of AGN	m	n	ρ	P
FWHM H β vs. Δz_{50} H β	209	2.90E-5 \pm 4.74E-5	1.85 \pm 0.19	0.69	P<0.00001
FW10%M H β vs. Δz_{10} H β	209	6.40E-5 \pm 1.14E-5	1.77 \pm 0.19	0.60	P<0.00001
FW5%M H β vs. Δz_5 H β	209	7.10E-5 \pm 1.39E-4	1.74 \pm 0.20	0.58	P<0.00001
FWHM Mg II vs. Δz_{50} Mg II	150	5.67E-6 \pm 1.31E-5	2.06 \pm 0.27	0.59	P<0.00001
FW10%M Mg II vs. Δz_{10} Mg II	150	1.26E+9 \pm 2.57E+9	-1.45 \pm 0.22	-0.62	P<0.00001
FW5%M Mg II vs. Δz_5 Mg II	150	2.133E+8 \pm 3.98E+8	-1.23 \pm 0.30	-0.68	P<0.00001
FWHM H β vs. Δz_{50} H β	123	5.74E-7 \pm 1.29E-6	2.33 \pm 0.25	0.78	P<0.00001
FWHM Mg II vs. Δz_{50} Mg II	123	1.37E-5 \pm 3.56E-5	1.96 \pm 0.30	0.53	P<0.00001

Table 2 The intrinsic redshifts and widths of Mg II (X) and H β lines (Y) are fitted with linear function: $Y = a \cdot X + b$. The parameters a and b , obtained from the fit, as well as the Spearman coefficients of correlation (ρ) and P -values, are also shown in the Table.

Mg II vs. H β	number of AGN	a	b	ρ	P
Δz_{50} Mg II vs. Δz_{50} H β	123	0.49 \pm 0.08	122.44 \pm 22.08	0.42	P<0.00001
Δz_{10} Mg II vs. Δz_{10} H β	123	0.10 \pm 0.08	791.65 \pm 120.10	0.10	P=0.22
Δz_5 Mg II vs. Δz_5 H β	123	0.07 \pm 0.08	936.05 \pm 134.50	0.10	P=0.38
FWHM Mg II vs. FWHM H β	123	0.80 \pm 0.08	1425.56 \pm 336.50	0.68	P<0.00001
FW10%M Mg II vs. FW10%M H β	123	0.02 \pm 0.06	10530.20 \pm 919.00	0.04	P= 0.78
FW5%M Mg II vs. FW5%M H β	123	-0.05 \pm 0.06	13878.90 \pm 994.30	-0.06	P= 0.36

A Appendix

Table 3 : Widths and shifts of the $H\beta$ line at half, 10% and 5% of the maximal intensity.

SDSS ID (MJD-plate-fiber)	FWHM $H\beta$ [km/s]	FW10%M $H\beta$ [km/s]	FW5%M $H\beta$ [km/s]	Δz_{50} $H\beta$ [km/s]	Δz_{10} $H\beta$ [km/s]	Δz_5 $H\beta$ [km/s]
51633-0268-235	4529	8512	9941	-47	-126	-203
51699-0349-613	3747	9488	11890	69	634	678
51703-0353-546	6529	20272	25188	25	224	224
51793-0402-479	4009	8735	10884	49	630	999
51817-0411-381	3496	9338	11409	-19	-276	-277
51817-0411-519	3197	8320	9966	21	124	124
51821-0408-611	2814	11601	14022	83	522	522
51821-0423-295	6557	12004	13622	701	1409	1557
51871-0409-213	2211	6113	7429	16	-12	-12
51873-0433-422	4614	9487	11127	108	367	394
51877-0385-061	3778	8932	10547	107	306	306
51883-0436-016	6903	14191	16293	660	1958	2192
51908-0464-576	7443	14499	16693	274	1078	1330
51910-0461-074	4153	9953	12288	71	803	926
51910-0465-603	2381	12448	14899	108	401	401
51913-0469-238	4926	12420	15046	159	774	786
51915-0453-212	6036	14233	16699	392	2075	2351
51929-0413-598	4248	12787	16809	36	719	729
51929-0490-126	5408	12397	14918	185	863	925
51930-0489-402	4862	10671	13095	2	-16	-20
51984-0498-104	3364	8791	11265	3	66	69
51989-0513-340	3251	7561	9416	52	668	901
51993-0551-179	5018	9569	11118	74	305	413
52000-0554-553	5669	12244	14371	316	1260	1416
52017-0366-584	4420	9737	11771	93	768	987
52026-0593-111	3747	8542	10322	67	386	414
52026-0593-170	4216	9645	11506	174	593	611
52045-0594-073	4046	8355	9906	32	149	170
52056-0329-577	4341	11489	13865	133	527	529
52056-0603-415	5763	15082	17206	400	3032	3445
52059-0597-337	3033	7988	9911	36	490	504
52059-0597-520	3206	8227	9887	27	174	175
52083-0628-461	3705	10004	12370	67	821	842
52143-0650-126	6655	12274	14009	219	578	682
52145-0625-288	6671	16539	19657	1045	2785	2800
52145-0653-185	2539	7354	9029	7	-33	-33
52148-0656-282	2960	9185	11733	47	1103	1129
52149-0666-024	1974	6471	8849	13	-61	-62
52149-0666-496	1704	7763	9692	11	-103	-103
52164-0634-430	6930	12407	14102	454	863	951
52173-0644-413	4297	11285	13751	-8	15	15
52174-0637-259	4689	9815	12162	27	312	497
52174-0664-455	3418	9476	11323	42	124	124
52178-0640-513	3552	7741	9156	125	865	1148
52201-0723-500	3620	8930	11169	-16	-169	-179

Table 3 : Table continued

SDSS ID (MJD-plate-fiber)	FWHM $H\beta$ [km/s]	FW10%M $H\beta$ [km/s]	FW5%M $H\beta$ [km/s]	Δz_{50} $H\beta$ [km/s]	Δz_{10} $H\beta$ [km/s]	Δz_5 $H\beta$ [km/s]
52224-0564-368	3754	10758	13049	97	532	533
52224-0564-471	3632	8346	11170	28	304	456
52224-0722-281	3398	8883	11061	39	464	477
52228-0721-454	2810	6056	7464	0	-38	-50
52233-0753-455	5617	11426	13278	134	292	297
52235-0755-225	4926	11468	13369	168	219	219
52238-0764-053	5121	12086	14408	304	1372	1461
52251-0752-020	5706	10397	11856	14	47	60
52252-0567-558	4510	9429	11368	69	345	438
52252-0767-300	3623	10938	13895	112	1732	1891
52252-0767-453	4497	9551	11272	142	833	1036
52261-0741-116	4324	9780	12292	-42	-201	-241
52266-0555-074	4295	9721	11626	181	696	739
52281-0768-085	1889	6867	8659	22	127	127
52295-0561-618	6590	13538	15956	191	898	1111
52312-0526-378	5871	10356	11665	354	684	758
52312-0827-621	3371	7995	9564	-128	-415	-421
52317-0600-490	3761	8231	9645	40	90	91
52319-0860-583	3639	7269	8421	468	983	1036
52339-0856-050	2580	8013	10530	-40	-167	-167
52353-0507-161	2854	11612	14654	72	1567	1567
52353-0792-116	7217	16992	19832	-191	-280	-280
52368-0607-581	3878	11275	14100	15	60	60
52370-0596-483	5453	11308	13802	38	136	182
52370-0793-549	5802	13914	17079	141	902	972
52370-0882-376	3879	10215	13047	41	343	356
52376-0773-629	2423	7856	10447	6	-355	-357
52376-0836-262	3109	7492	10063	-36	-450	-620
52378-0795-381	5178	10396	12103	217	777	927
52378-0795-528	3377	9448	11829	9	215	217
52378-0892-395	3801	8805	11930	32	16	8
52378-0916-434	6742	11616	13034	670	1161	1278
52381-0510-509	2986	9821	12448	47	488	488
52413-0976-574	2048	6217	8793	13	-176	-181
52442-0984-383	6582	11810	13269	578	1159	1266
52443-0814-467	6461	12249	14130	-20	-26	-27
52466-1052-370	2299	4598	5735	23	170	367
52516-1054-309	4917	10524	12220	111	175	175
52521-0738-095	4473	15273	19349	113	3141	3531
52523-0987-157	2581	7902	10506	-48	-452	-457
52592-0896-063	4429	9538	11232	237	740	778
52605-0897-242	2948	9028	11600	22	411	413
52620-0899-626	2917	8665	11764	25	-50	-52
52620-0932-110	5442	11317	15230	37	669	1810
52636-0511-567	3051	7527	9269	40	153	158
52636-0939-172	6371	12590	14535	286	1021	1210
52636-0967-044	6649	12368	14203	79	325	428
52636-0999-334	5140	10751	12743	17	-30	-36
52642-0837-298	2773	9040	11121	99	912	913

Table 3 : Table continued

SDSS ID (MJD-plate-fiber)	FWHM H β [km/s]	FW10%M H β [km/s]	FW5%M H β [km/s]	Δz_{50} H β [km/s]	Δz_{10} H β [km/s]	Δz_5 H β [km/s]
52646-1186-098	4478	11183	13065	468	523	523
52669-0848-418	4564	11445	13422	115	204	204
52672-1230-503	2343	5121	7676	-44	-256	-798
52674-1201-225	2356	5545	8399	9	65	114
52703-0942-488	3042	8909	11852	-11	-588	-606
52703-1005-518	3187	8577	10814	41	132	134
52703-1199-596	3328	9042	11210	7	-71	-71
52709-0941-616	6584	15207	17746	378	2169	2530
52709-1218-201	3878	9018	11240	-22	25	32
52710-0993-147	2144	7820	9662	-6	-391	-391
52721-0914-074	3556	8730	10399	97	359	361
52723-1004-280	4949	11156	13092	76	150	150
52724-1195-098	4407	9371	10950	639	1020	1022
52725-0994-086	3045	7858	9840	19	145	149
52725-1215-150	3049	6424	8448	-17	-114	-245
52731-1214-077	3899	8610	10421	19	57	62
52731-1214-160	5346	11130	13036	129	367	381
52738-1167-476	3799	10704	12937	-21	-240	-240
52753-1171-416	4873	9913	11983	49	428	668
52762-1237-497	3468	7387	9490	-18	76	156
52765-1224-379	3095	9399	11980	24	292	293
52767-1329-542	4453	10882	13004	97	1581	2087
52781-1223-625	2608	8053	10055	-1	-23	-24
52790-1351-428	6439	11669	13300	566	1040	1128
52793-1342-157	5073	9870	11340	350	387	387
52821-1371-377	4900	9964	11563	299	498	501
52872-1402-594	1968	7401	9517	-29	-324	-324
52974-1271-462	3226	8777	10531	-146	-657	-658
52990-1429-584	4877	13393	15851	479	1024	1024
52990-1592-018	6449	12038	13730	274	742	873
52992-1431-572	4412	10629	13126	-103	-1150	-1468
52993-1273-348	5952	12179	14149	926	1995	2089
52996-1427-606	3707	9349	11192	198	855	864
52998-1428-558	3537	9744	12108	83	845	865
53003-1432-091	4827	11130	13577	-98	-734	-830
53033-1310-559	4441	8705	10279	36	137	185
53033-1598-291	4171	9163	11367	20	-34	-49
53033-1598-604	3280	6864	8687	27	150	260
53035-1433-148	2706	7530	10569	6	-250	-270
53035-1735-322	3665	7557	9190	44	399	627
53050-1362-119	3418	9073	11251	58	261	264
53055-1606-166	2974	8139	10405	-1	-319	-327
53055-1744-387	4022	8769	10349	35	148	152
53061-1364-185	3593	8754	10174	142	1388	1666
53061-1378-413	3083	8435	10468	43	1460	2047
53061-1378-488	2968	7957	10520	-16	41	44
53062-1372-488	4403	10958	13859	60	1457	2200
53078-1604-281	3594	7707	9975	14	96	165
53080-1446-135	6623	15943	18557	420	2574	2969

Table 3 : Table continued

SDSS ID (MJD-plate-fiber)	FWHM $H\beta$ [km/s]	FW10%M $H\beta$ [km/s]	FW5%M $H\beta$ [km/s]	Δz_{50} $H\beta$ [km/s]	Δz_{10} $H\beta$ [km/s]	Δz_5 $H\beta$ [km/s]
53083-1367-629	4913	11283	13789	95	668	754
53084-1380-058	6258	11508	13171	64	179	228
53084-1440-137	3739	9581	12040	27	523	554
53084-1453-010	5534	14434	17698	167	2177	2782
53084-1619-060	5505	12617	15061	140	562	578
53089-1455-584	6634	11923	13323	689	1304	1378
53089-1779-106	3437	10220	13141	26	648	655
53108-1394-044	4423	8836	10703	-24	-120	-195
53112-1773-301	4652	11691	13766	-70	-141	-141
53112-1773-405	2320	7144	10141	-5	299	306
53116-1457-421	3863	8915	11243	-57	-432	-528
53119-1603-558	5499	10275	11889	1009	1436	1444
53141-1417-441	5363	10654	12432	170	610	733
53147-1676-055	3479	9239	12704	13	619	725
53172-1645-526	5824	11780	13690	158	323	330
53228-1728-218	2805	6838	9219	-13	205	266
53312-1865-572	3440	9429	12900	44	1576	2777
53313-1864-353	4467	10215	12264	20	133	138
53317-1926-378	2749	7140	9574	-23	-467	-542
53350-2080-309	3709	8866	11182	-16	-262	-295
53358-1750-564	4986	10935	12981	163	927	1066
53383-1940-407	7203	14543	16783	404	502	502
53385-1754-324	3171	9330	12310	39	187	188
53385-1944-412	3290	9093	11017	70	265	265
53386-1872-371	3946	11269	13944	163	1688	1810
53386-1941-545	3730	9149	11905	52	508	603
53430-1667-114	3736	9470	11546	-76	-573	-586
53431-2020-614	6260	13653	15805	439	439	439
53433-1949-437	2983	8754	10518	13	-14	-14
53433-1949-472	1855	9323	13225	37	1847	1850
53436-1683-016	4877	15006	17883	106	3179	3897
53437-0614-452	3132	7694	10396	4	444	596
53442-2003-501	3267	7539	9672	18	352	469
53466-2034-230	3729	8693	10578	28	220	233
53467-1838-451	6517	13961	16390	-117	-358	-365
53472-1626-449	3992	12120	14942	104	2259	2653
53472-1694-540	3108	6500	8659	-26	-75	-160
53473-1695-612	2310	7193	9909	-47	-575	-588
53473-2008-615	3332	8648	10544	106	601	610
53474-2007-171	5446	14432	16359	308	2885	3250
53474-2007-226	3296	11160	13845	-44	-415	-415
53475-1690-634	6060	13950	16990	181	1167	1369
53493-1575-484	2039	6919	8481	-58	-300	-300
53498-2089-385	9030	16304	18540	566	1137	1265
53499-2030-201	5754	11939	13971	168	1067	1375
53521-1714-011	3642	13992	18377	77	1967	1972
53521-1714-571	3783	9825	12029	103	637	649
53566-1854-151	2916	8035	11041	4	909	1170
53674-2265-087	3312	8936	11112	42	533	544

Table 3 : Table continued

SDSS ID (MJD-plate-fiber)	FWHM H β [km/s]	FW10%M H β [km/s]	FW5%M H β [km/s]	Δz_{50} H β [km/s]	Δz_{10} H β [km/s]	Δz_5 H β [km/s]
53711-2281-431	5194	10037	11582	168	598	715
53712-2276-508	3472	8168	12484	17	649	1765
53713-2292-348	6651	14092	16454	530	1012	1017
53714-2106-130	4083	8154	9722	62	431	661
53733-2294-607	4488	11389	13440	-444	-913	-913
53737-2364-469	2714	6131	8139	23	9	1
53738-2341-066	3235	8168	10453	42	241	257
53739-2365-591	2813	8372	10868	-4	-442	-447
53757-2347-151	3522	12496	15725	78	2782	3226
53757-2347-326	4386	9485	11343	66	381	425
53759-2362-295	3372	8477	10805	-3	295	322
53770-2352-242	3645	9633	12624	72	751	832
53770-2376-497	2399	6528	8630	10	40	41
53772-1989-559	1583	6753	8811	-30	-198	-198
53772-2351-099	4924	11437	13787	-62	-376	-392
53772-2351-616	4035	8335	9995	6	137	177
53794-1810-504	3080	8472	11020	16	-99	-102
53794-2353-600	4276	9578	11524	117	665	748
53795-2216-298	4100	10627	12740	273	1586	1685
53799-2222-388	4570	11474	13782	114	1729	2247
53800-2128-415	3620	8258	10658	-6	-11	-12
53801-2428-356	6023	15080	18181	295	1942	2130
53816-1843-008	3104	8339	10004	-60	-254	-255
53816-1843-502	4866	10313	12797	-70	-426	-634
53816-1843-584	4100	9768	12374	66	855	1139
53818-2440-539	5538	15199	18502	265	2316	2504
53827-1713-063	4729	12519	15393	118	1050	1078
53827-1716-350	5427	13849	16481	-136	-372	-372
53828-2237-093	4439	8636	9964	308	456	458
53845-2233-196	5268	12601	14816	-7	-24	-24
53847-1775-420	2858	8752	12531	-30	-1052	-1170
53851-1817-069	3059	5585	6378	11	11	11
53851-2023-065	3306	10428	13413	-5	-92	-92
53855-2491-252	5542	14495	16840	303	2681	3108
53858-2101-348	2532	7408	9796	22	-129	-131
53874-2152-108	4647	10771	13112	124	821	928
53874-2173-354	4232	9454	11657	90	534	658
53875-2508-353	4565	8328	9464	104	304	355
53877-2512-582	5554	11821	14166	121	865	1144
53883-1793-573	3354	11508	15301	87	2133	2321
53884-1796-591	6373	12584	14563	685	1487	1570
53886-2164-503	3605	9520	11512	65	455	457
54084-2501-120	4594	11143	13378	193	900	923
54086-2420-240	3985	10047	12181	21	175	177
54095-2583-462	3675	8779	10676	22	96	99
54095-2583-615	2966	9194	11611	64	434	434
54097-2478-377	2376	7985	10703	5	-337	-338
54115-2102-018	4020	9604	11320	123	299	299
54115-2493-278	3952	8670	11756	6	270	567

Table 3 : Table continued

SDSS ID (MJD-plate-fiber)	FWHM $H\beta$ [km/s]	FW10%M $H\beta$ [km/s]	FW5%M $H\beta$ [km/s]	Δz_{50} $H\beta$ [km/s]	Δz_{10} $H\beta$ [km/s]	Δz_5 $H\beta$ [km/s]
54138-1844-112	5449	10751	12477	172	770	991
54139-2425-442	5851	14929	17564	559	2712	2910
54144-1845-637	6106	14792	17466	128	328	328
54149-2488-521	4555	14749	18427	97	1167	1168
54152-1803-323	5269	11049	12612	387	1483	1708
54153-2242-199	4894	10187	12351	-45	-205	-266
54154-2606-614	3426	9002	11900	-36	-573	-637
54175-1807-009	2316	6996	8787	-10	-37	-37
54176-1847-630	4231	8969	10912	32	221	282
54176-2485-231	10334	18710	21287	411	937	1066
54178-2492-562	5270	9605	10957	2	2	3
54178-2592-153	3410	8351	10949	-1	342	414
54180-2509-244	3618	8947	11372	39	1007	1429
54207-2595-541	5342	9998	11435	182	556	668
54230-2641-570	5124	11213	13331	185	825	911
54232-2166-030	2423	7033	9706	-46	-455	-475
54243-2518-374	3694	11319	13489	241	2369	2549
54266-1725-540	2861	9653	11847	86	539	539
54266-1791-046	2527	8216	11470	13	166	167
54272-2744-535	2554	7816	11029	-9	-616	-643
54448-2424-109	2019	8864	11050	38	484	484
54477-2645-133	3788	9030	11006	80	349	364
54479-2646-204	4692	10819	12705	225	1431	1688
54481-2613-620	2492	6170	9247	-26	24	47
54483-2615-257	2218	6423	8375	24	-130	-132
54483-2615-404	3303	11501	14611	109	1619	1629
54495-2647-160	5341	11647	14659	10	214	303
54497-2885-561	4663	8732	9981	142	464	562
54502-2617-287	2819	7185	8829	78	430	441
54507-1795-509	3777	12110	13977	107	2816	3287
54523-2151-527	2305	7501	9879	19	586	590
54524-2783-432	4980	9280	10507	353	888	1006
54527-2769-354	2948	9305	12477	-17	-292	-294
54529-2772-038	3151	8809	11521	16	804	867
54534-2774-051	7294	14911	17025	727	2158	2431
54535-2764-053	3093	8250	10684	45	713	785
54562-2955-608	3447	8698	11256	-23	-37	-38
54563-2795-140	6120	12639	14694	655	1001	1003
54567-2517-624	2293	8041	9969	2	-237	-237
54570-2522-131	4064	10894	14375	76	1781	2911
54582-2526-404	3706	8232	10260	34	597	895
54584-2520-442	6040	13853	16167	841	1095	1095
54585-2529-300	3514	9254	11842	17	315	328
54589-2532-090	4530	10194	12457	92	776	978
54589-2970-373	3194	10759	13867	64	993	995
54590-2971-326	2342	7923	10079	39	242	242

Table 4 : Widths and shifts of the Mg II line at half, 10% and 5% of the maximal intensity.

SDSS ID (MJD-plate-fiber)	FWHM Mg II [km/s]	FW10%M Mg II [km/s]	FW5%M Mg II [km/s]	Δz_{50} Mg II [km/s]	Δz_{10} Mg II [km/s]	Δz_5 Mg II [km/s]
51633-0268-235	4951	17580	24989	44	297	297
51699-0349-613	2875	24042	24579	40	605	605
51703-0353-546	6566	21014	24335	-79	-337	-336
51793-0402-479	3617	14447	23860	-58	-762	-762
51817-0411-381	3059	14447	25233	25	545	545
51817-0411-519	3139	21863	21923	-3	1157	1157
51821-0408-611	3123	21874	21310	-1	-947	-947
51821-0423-295	6051	20659	15409	1410	2150	2150
51871-0409-213	2120	20418	19894	-15	368	368
51873-0433-422	4085	18678	14447	226	2198	2379
51877-0385-061	3450	26471	21818	37	260	260
51883-0436-016	4409	23526	16296	240	2853	3140
51908-0464-576	4639	26920	16555	345	2030	2047
51910-0461-074	4377	14606	25667	60	773	774
51910-0465-603	4085	21535	14447	226	2198	2379
51913-0469-238	5032	25193	22310	47	235	235
51915-0453-212	6747	21299	17121	419	1861	2140
51929-0413-598	3368	14447	12869	104	2413	2793
51929-0490-126	4095	14447	14364	182	2457	2827
51930-0489-402	4596	16612	28439	-51	-679	-679
51984-0498-104	3016	25830	14192	25	339	340
51989-0513-340	4085	24166	14447	226	2198	2379
51993-0551-179	4091	19083	23680	23	212	212
52000-0554-553	5011	26218	22152	6	270	270
52017-0366-584	4085	24263	14447	226	2198	2379
52026-0593-111	3279	14155	12749	70	1410	1536
52026-0593-170	3067	14517	14367	64	2696	2941
52045-0594-073	3322	19302	18898	-31	-241	-241
52056-0329-577	4085	23311	14447	226	2198	2379
52056-0603-415	5869	20308	14948	294	1803	2079
52059-0597-337	2894	21500	23123	66	1763	1763
52059-0597-520	2422	13115	19016	6	15	16
52083-0628-461	2892	15223	21336	11	194	194
52143-0650-126	5809	18844	21391	-8	-102	-103
52145-0625-288	4649	24047	17240	277	2550	2654
52145-0653-185	1831	25772	11428	-3	691	926
52148-0656-282	2337	22659	10803	62	2109	2623
52149-0666-024	2307	21106	24398	11	836	836
52149-0666-496	2204	20249	22611	-14	-338	-338
52164-0634-430	4604	24563	13731	333	2414	2744
52173-0644-413	4085	24247	23098	-80	-1527	-1526
52174-0637-259	3382	23226	24350	24	-240	-240
52174-0664-455	3196	20882	26189	8	47	47
52178-0640-513	3266	24635	14608	128	2390	2517
52201-0723-500	2929	24095	20385	6	-776	-775
52224-0564-368	4085	19846	14447	226	2198	2379
52224-0564-471	4085	18836	14447	226	2198	2379
52224-0722-281	3704	21399	19450	-11	-308	-308

Table 4 : Table continued

SDSS ID (MJD-plate-fiber)	FWHM Mg II [km/s]	FW10%M Mg II [km/s]	FW5%M Mg II [km/s]	Δz_{50} Mg II [km/s]	Δz_{10} Mg II [km/s]	Δz_5 Mg II [km/s]
52228-0721-454	2819	21596	25271	23	-524	-524
52233-0753-455	4085	18816	14447	226	2198	2379
52235-0755-225	4085	24636	14447	226	2198	2379
52238-0764-053	4621	22038	21259	55	453	454
52251-0752-020	4395	21767	26138	14	-91	-91
52252-0567-558	3597	21087	23643	38	520	521
52252-0767-300	4933	14383	23536	72	188	188
52252-0767-453	3862	12732	23907	-21	-697	-697
52261-0741-116	4113	26062	22213	-93	-1383	-1383
52266-0555-074	3894	26002	13288	198	1892	2057
52281-0768-085	2193	22518	19718	-1	468	469
52295-0561-618	5927	18057	13415	472	1117	1212
52312-0526-378	3766	14447	21367	-12	-243	-242
52312-0827-621	2031	21922	21849	-29	-574	-575
52317-0600-490	2964	22361	14306	23	1510	1523
52319-0860-583	2980	20824	26633	-16	-83	-83
52339-0856-050	2348	16346	23580	-39	-1504	-1504
52353-0507-161	3077	17594	19279	-23	6	6
52353-0792-116	2964	20911	20001	-26	-244	-244
52368-0607-581	4090	19162	21729	-20	73	72
52370-0596-483	4781	20372	21926	-33	-156	-156
52370-0793-549	4398	19409	22810	10	69	69
52370-0882-376	2444	17308	20347	-29	-679	-679
52376-0773-629	2070	19174	17857	7	-882	-883
52376-0836-262	2711	21614	20254	7	265	265
52378-0795-381	4681	14495	25020	2	354	354
52378-0795-528	3368	22527	21709	-52	-794	-794
52378-0892-395	4046	21747	19897	46	505	506
52378-0916-434	5082	25260	15374	309	1736	1820
52381-0510-509	2945	23911	18564	-13	-941	-941
52413-0976-574	1862	21586	16958	-24	677	677
52442-0984-383	5561	20362	24043	70	321	321
52443-0814-467	3711	10624	22278	-25	-388	-388
52466-1052-370	4085	19336	14447	226	2198	2379
52516-1054-309	4125	16115	26033	-68	-444	-444
52521-0738-095	4085	24059	14447	226	2198	2379
52523-0987-157	2472	9864	21124	-26	-1749	-1749
52592-0896-063	4219	19010	23391	6	273	273
52605-0897-242	2478	28281	21585	3	215	215
52620-0899-626	2865	12879	26912	6	-247	-247
52620-0932-110	5192	22851	25566	0	-175	-175
52636-0511-567	2610	20783	21977	14	-852	-852
52636-0939-172	6681	26792	23683	8	32	32
52636-0967-044	3707	24120	13567	83	1546	1661
52636-0999-334	4927	20947	13650	229	1859	2214
52642-0837-298	3594	23403	15590	101	2252	2343
52646-1186-098	3995	23614	12530	153	1685	1990
52669-0848-418	4062	19350	15026	216	2138	2234
52672-1230-503	2542	24608	19098	34	221	221

Table 4 : Table continued

SDSS ID (MJD-plate-fiber)	FWHM Mg II [km/s]	FW10%M Mg II [km/s]	FW5%M Mg II [km/s]	Δz_{50} Mg II [km/s]	Δz_{10} Mg II [km/s]	Δz_5 Mg II [km/s]
52674-1201-225	2056	21762	20719	14	-146	-147
52703-0942-488	2430	20461	20325	4	1890	1891
52703-1005-518	2883	14515	21125	-55	-1172	-1172
52703-1199-596	2304	21343	17580	-30	495	496
52709-0941-616	4031	19856	24042	-41	-222	-222
52709-1218-201	3035	19231	21014	-20	-830	-830
52710-0993-147	4085	22895	14447	226	2198	2379
52721-0914-074	4085	19744	14447	226	2198	2379
52723-1004-280	3572	20407	21863	-61	-1249	-1249
52724-1195-098	3663	22393	21874	-7	31	31
52725-0994-086	2201	23650	20659	-4	282	281
52725-1215-150	2274	19637	20418	-35	-952	-951
52731-1214-077	2981	12216	18678	-54	-2771	-2879
52731-1214-160	3503	22134	26471	-19	14	14
52738-1167-476	3623	21070	23526	18	423	422
52753-1171-416	4574	13105	26920	-95	-835	-834
52762-1237-497	3468	21034	14606	64	1465	1503
52765-1224-379	3273	22946	21535	-35	-275	-274
52767-1329-542	3503	23493	25193	7	315	315
52781-1223-625	3078	15589	21299	23	-303	-303
52790-1351-428	4085	22599	14447	226	2198	2379
52793-1342-157	4085	19620	14447	226	2198	2379
52821-1371-377	3733	23656	16612	196	2366	2372
52872-1402-594	2100	20726	25830	-30	-884	-884
52974-1271-462	2528	23159	24166	-18	1227	1227
52990-1429-584	4391	25508	19083	69	1020	1021
52990-1592-018	3394	18676	26218	-45	-557	-558
52992-1431-572	3211	25084	24263	33	-32	-31
52993-1273-348	5782	13282	14155	998	2153	2225
52996-1427-606	4779	21926	14517	347	2715	3040
52998-1428-558	3339	25580	19302	12	-553	-553
53003-1432-091	4852	18929	23311	-80	-678	-679
53033-1310-559	4013	17747	20308	-66	-1435	-1435
53033-1598-291	4623	19081	21500	66	926	926
53033-1598-604	2912	16970	13115	43	759	759
53035-1433-148	2117	18800	15223	7	292	292
53035-1735-322	2752	12832	18844	-20	880	880
53050-1362-119	3065	15254	24047	-33	-290	-291
53055-1606-166	3074	11951	25772	-6	453	453
53055-1744-387	3766	21672	22659	-18	-665	-665
53061-1364-185	3320	11669	21106	2	508	509
53061-1378-413	2635	16515	20249	16	-626	-626
53061-1378-488	2891	21821	24563	-6	334	335
53062-1372-488	3909	33760	24247	2	-736	-736
53078-1604-281	2648	15143	23226	0	-661	-661
53080-1446-135	4649	15906	20882	-30	-273	-273
53083-1367-629	3890	19109	24635	1	-7	-6
53084-1380-058	6749	10569	24095	-68	-261	-261
53084-1440-137	2623	21326	19846	-39	-731	-731

Table 4 : Table continued

SDSS ID (MJD-plate-fiber)	FWHM Mg II [km/s]	FW10%M Mg II [km/s]	FW5%M Mg II [km/s]	Δz_{50} Mg II [km/s]	Δz_{10} Mg II [km/s]	Δz_5 Mg II [km/s]
53084-1453-010	3168	21937	18836	4	200	200
53084-1619-060	3808	20902	21399	-9	215	215
53089-1455-584	4355	20815	21596	6	137	137
53089-1779-106	3310	19409	18816	15	-381	-381
53108-1394-044	3192	25958	24636	-2	721	721
53112-1773-301	3122	24010	22038	27	459	459
53112-1773-405	2404	23418	21767	1	131	132
53116-1457-421	3574	12726	21087	-20	-435	-436
53119-1603-558	4470	20642	14383	434	2511	2680
53141-1417-441	4806	13114	12732	189	1413	1751
53147-1676-055	2767	21841	26062	23	319	320
53172-1645-526	6731	19818	26002	-25	-101	-101
53228-1728-218	2558	24090	22518	-28	379	379
53312-1865-572	1831	24033	18057	4	687	687
53313-1864-353	4085	22208	14447	226	2198	2379
53317-1926-378	2703	19486	21922	-16	-164	-164
53350-2080-309	3243	13309	22361	20	-44	-43
53358-1750-564	4111	12876	20824	60	395	395
53383-1940-407	6341	23989	16346	476	1591	1698
53385-1754-324	2365	19889	17594	21	877	877
53385-1944-412	3680	22540	20911	9	614	614
53386-1872-371	3852	15745	19162	10	114	114
53386-1941-545	2722	26586	20372	-3	-1024	-1023
53430-1667-114	2951	26141	19409	17	584	584
53431-2020-614	4586	21896	17308	325	902	902
53433-1949-437	2264	21479	19174	15	345	345
53433-1949-472	6425	12423	21614	1047	1362	1363
53436-1683-016	5020	14880	14495	228	1424	1549
53437-0614-452	2706	16580	22527	22	322	321
53442-2003-501	2600	22415	21747	-12	462	462
53466-2034-230	3416	25741	25260	24	131	131
53467-1838-451	3625	21764	23911	19	-7	-7
53472-1626-449	3940	22901	21586	23	682	682
53472-1694-540	2383	21982	20362	-1	714	714
53473-1695-612	2070	22099	10624	17	2562	3188
53473-2008-615	2747	23874	19336	16	136	135
53474-2007-171	4934	14496	16115	309	1702	1729
53474-2007-226	2743	12863	24059	-29	259	259
53475-1690-634	3482	21944	9864	538	1580	1615
53493-1575-484	2322	14476	19010	30	775	776
53498-2089-385	8503	19455	28281	279	1165	1166
53499-2030-201	4620	10898	12879	728	1991	2035
53521-1714-011	3366	17366	22851	10	-598	-598
53521-1714-571	3583	16781	20783	-5	-255	-254
53566-1854-151	3254	21235	26792	-7	-322	-321
53674-2265-087	3611	18850	24120	-25	-580	-580
53711-2281-431	4923	17370	20947	67	286	286
53712-2276-508	3236	17362	23403	-32	-769	-770
53713-2292-348	5760	19793	23614	-205	-596	-596

Table 4 : Table continued

SDSS ID (MJD-plate-fiber)	FWHM Mg II [km/s]	FW10%M Mg II [km/s]	FW5%M Mg II [km/s]	Δz_{50} Mg II [km/s]	Δz_{10} Mg II [km/s]	Δz_5 Mg II [km/s]
53714-2106-130	2280	13043	19350	-4	724	724
53733-2294-607	2217	17652	24608	19	961	962
53737-2364-469	2290	13798	21762	21	-103	-103
53738-2341-066	2835	15746	20461	16	19	19
53739-2365-591	2382	10312	14515	-13	1359	1361
53757-2347-151	2894	16159	21343	8	-216	-216
53757-2347-326	3197	15542	19856	16	345	345
53759-2362-295	1998	12669	19231	-16	1308	1308
53770-2352-242	3357	17929	22895	-22	128	128
53770-2376-497	2619	13949	19744	7	141	141
53772-1989-559	1956	13120	20407	17	-743	-744
53772-2351-099	3441	16890	22393	36	510	511
53772-2351-616	4257	18800	23650	19	83	83
53794-1810-504	2991	14673	19637	-18	-344	-344
53794-2353-600	3115	10301	12216	92	2408	2901
53795-2216-298	3334	17934	22134	-16	-178	-178
53799-2222-388	3109	16042	21070	3	-567	-568
53800-2128-415	3260	11089	13105	106	2672	3172
53801-2428-356	4260	17357	21034	-49	-342	-342
53816-1843-008	3214	17328	22946	-9	-507	-507
53816-1843-502	3731	19401	23493	-36	-558	-559
53816-1843-584	3188	12348	15589	89	1960	1964
53818-2440-539	5832	18680	22599	40	368	368
53827-1713-063	3072	16202	19620	40	299	299
53827-1716-350	4097	19387	23656	-29	-257	-257
53828-2237-093	3131	16441	20726	0	220	220
53845-2233-196	3322	18757	23159	-44	-621	-620
53847-1775-420	2378	18475	25508	20	-45	-45
53851-1817-069	1992	12907	18676	40	1154	1154
53851-2023-065	2407	18911	25084	-12	-1364	-1364
53855-2491-252	3857	10980	13282	222	1729	1781
53858-2101-348	2364	15837	21926	11	-178	-178
53874-2152-108	4483	20349	25580	-5	-282	-282
53874-2173-354	4425	15002	18929	0	105	105
53875-2508-353	2609	12370	17747	-18	1368	1368
53877-2512-582	4530	14909	19081	53	1035	1037
53883-1793-573	2636	12781	16970	44	1612	1612
53884-1796-591	4871	15675	18800	161	746	746
53886-2164-503	3524	10830	12832	134	2278	2609
54084-2501-120	3469	12275	15254	116	1564	1565
54086-2420-240	2094	9655	11951	67	2842	3384
54095-2583-462	3192	16993	21672	1	-257	-256
54095-2583-615	2661	9378	11669	123	2019	2148
54097-2478-377	1889	8287	16515	23	262	262
54115-2102-018	3390	16757	21821	-21	-175	-175
54115-2493-278	3222	18640	33760	-19	-284	-5224
54138-1844-112	3773	12483	15143	193	1129	1129
54139-2425-442	4915	13077	15906	227	1465	1502
54144-1845-637	4159	15735	19109	-32	-279	-279

Table 4 : Table continued

SDSS ID (MJD-plate-fiber)	FWHM Mg II [km/s]	FW10%M Mg II [km/s]	FW5%M Mg II [km/s]	Δz_{50} Mg II [km/s]	Δz_{10} Mg II [km/s]	Δz_5 Mg II [km/s]
54149-2488-521	3240	8994	10569	154	1711	1958
54152-1803-323	3733	16984	21326	-15	-159	-158
54153-2242-199	3262	17364	21937	-59	-1563	-1563
54154-2606-614	3091	16227	20902	21	229	229
54175-1807-009	2546	14708	20815	2	1049	1049
54176-1847-630	3521	15330	19409	3	-261	-261
54176-2485-231	6537	21678	25958	-156	-602	-602
54178-2492-562	5245	19656	24010	-72	-524	-524
54178-2592-153	2310	17164	23418	7	-553	-552
54180-2509-244	3607	10674	12726	159	2145	2505
54207-2595-541	4036	15870	20642	41	830	831
54230-2641-570	3999	10882	13114	182	1742	1916
54232-2166-030	3003	17051	21841	67	3678	3678
54243-2518-374	3843	16080	19818	104	1230	1231
54266-1725-540	2636	17294	24090	9	1055	1055
54266-1791-046	2225	16680	24033	20	-1356	-1355
54272-2744-535	1978	14196	22208	-28	-686	-685
54448-2424-109	2688	15162	19486	14	-296	-297
54477-2645-133	2916	10247	13309	92	2049	2218
54479-2646-204	3146	11068	12876	127	2787	3139
54481-2613-620	2418	17430	23989	-23	1054	1054
54483-2615-257	2074	12173	19889	-30	-468	-468
54483-2615-404	2816	17082	22540	-25	230	229
54495-2647-160	4420	13133	15745	158	661	660
54497-2885-561	3315	20523	26586	16	334	334
54502-2617-287	3000	18933	26141	-14	1160	1160
54507-1795-509	3421	17250	21896	-15	-837	-837
54523-2151-527	2704	15579	21479	-33	-513	-514
54524-2783-432	4446	10601	12423	183	1538	1839
54527-2769-354	2665	11186	14880	69	2634	2777
54529-2772-038	2515	10850	16580	-8	1557	1563
54534-2774-051	6160	18785	22415	-116	-372	-372
54535-2764-053	2525	19802	25741	27	-481	-482
54562-2955-608	3898	16919	21764	-75	-1200	-1199
54563-2795-140	4374	18846	22901	-48	-279	-280
54567-2517-624	2748	16077	21982	2	311	312
54570-2522-131	4061	17375	22099	8	-514	-514
54582-2526-404	3370	17926	23874	-14	-328	-328
54584-2520-442	3932	12126	14496	554	1869	1870
54585-2529-300	2687	9822	12863	23	1699	1740
54589-2532-090	4495	17861	21944	69	695	695
54589-2970-373	3373	11772	14476	87	2681	3143
54590-2971-326	3282	14706	19455	32	805	806